APPLICATIONS OF LOW-PRESSURE GASEOUS MULTIWIRE DETECTORS TO MEASUREMENT OF ANGULAR DISTRIBUTIONS OF NUCLEAR FISSION FRAGMENTS AND FOR MONITORING OF NEUTRON BEAM PROFILE AT NEUTRON TOF-SPECTROMETER GNEIS

A.M. Gagarski, A.S. Vorobyev, O.A. Shcherbakov, L.A. Vaishnene

NRC "Kurchatov Institute", B.P. Konstantinov Petersburg Nuclear Physics Institute, 188300, Gatchina, Russia

Abstract

Low-pressure gaseous multiwire proportional counters (LPMWPC) are known as simple, efficient and low cost transmission timing detectors for heavy ions. In the presented work we describe applications of such detection systems for study of fission fragments angular distributions in fission induced by 1-200 MeV neutrons at neutron spectrometer GNEIS (PNPI, Gatchina, Russia). Another application of LPMWPCs as neutron beam space profile monitor at the electronic devices radiation resistance test facility ISNP/GNEIS in Gatchina is also discussed.

1. Basic principles, main characteristics of LPMWPC and the detector construction

Conventional gaseous multiwire proportional counters (MWPC) were invented at least in 1970 [1] and are widely used since that time. Slightly later, it was shown [2,3] that at low pressure and high reduced electric field (E/p – electric field divided to pressure) the MWPCs possess excellent timing properties. Review of such low-pressure MWPCs (LPMWPC) was given in [4].

The specific properties of LPMWPC are resulted from the fact that at low pressures the reduced electric field become high enough for secondary ionization to be produced even in the homogeneous field region (see Fig.1). The amplification is exponentially dependent on the drift length. Therefore, the electrons from the part of the track closest to the cathode will have maximum amplification and thus practically only this part of the track will define start of anode signal. A point of interaction (close to cathode) becomes well localized and time resolution better than 1 ns can be achieved. In vicinity of the anode wires (~0.1 mm around the wire), another stage of amplification will occur like in conventional MWPC. It should be noted that in this case there will be no significant spreading of signal between many wires even for oblique tracks, because only the point of the track near cathode will gain maximum amplification and the main signal will be induced only on the wire in front of this point. The precise coordinate information can be obtained by making proper signal readout of individual anode wires.

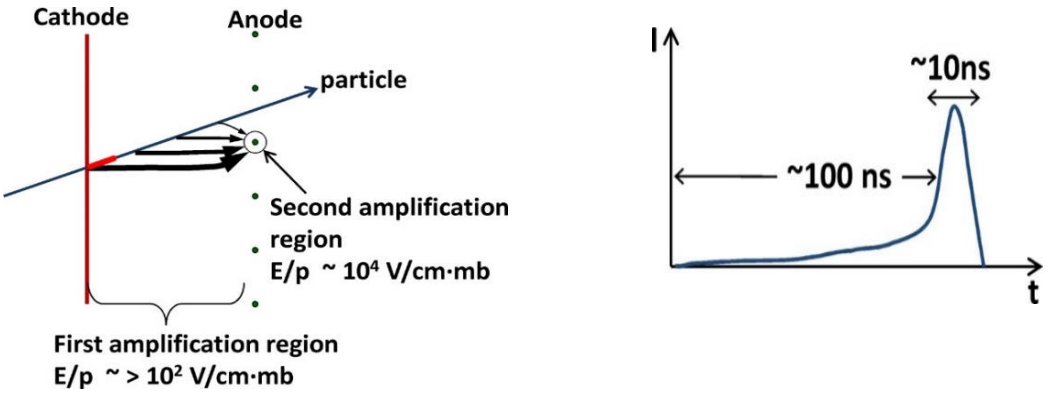

Fig. 1. Illustration of operational principle of LPMWPC (left) and typical current signal shape (right).

Basic advantages of LPMWPCs which make them very suitable for registration of heavy ions such as fission fragments (FFs) are the following: excellent timing characteristics, high efficiency, high transparency and low energy losses inside the detector, large surface area, high counting rate capability, good position resolution with proper signal readout, long term stability. The table below contains typical parameters of LPMWPCs:

Working pressure:	~0.1–10 mbar
Counting gases:	isobutane, heptane, ethylene
Anode–cathode gap:	~1.6–3.2 mm
Anode wire spacing:	~1 mm
Anode wire diameter:	~10–25 μm
Reduced electric field in the constant field region:	~10^2–10^3 V/(cm·mb)
Reduced electric field on the wire surface:	~10^4–10^5 V/(cm·mb)
Total gas amplification:	~10^4–10^6
Amplification on the wires:	~10^1–10^3
Signal current pulses rise time:	~2–5 ns
Timing resolution	~0.1–1 ns

The schema of position sensitive transparent detector for FFs developed for our experiments is shown in Fig. 2 Each detector consists of X and Y anodes wire planes made of ⌀25 μm gilded tungsten wires. The cathode is made as a square mesh from the same wire. The wire spacing is 1 mm, and both gaps are ~3.2 mm. The detectors operate with isobutane as a counting gas at ~8 mb pressure. Voltage ~560–600 V is applied to common cathode. Total area of the detector is 140×140 mm^2. The 140 anode wires are connected by pairs to 70 taps of delay lines (50 Ω impedance, 2 ns per tap). One end of each delay is grounded and timing signals taken from another end of the delay carry position information (T_X, T_Y). Timing signal is taken from cathode plane (T_0). The coordinates are proportional to the time differences between cathode and anode signals. Typical digitized anode signals from FFs are shown in Fig. 3.

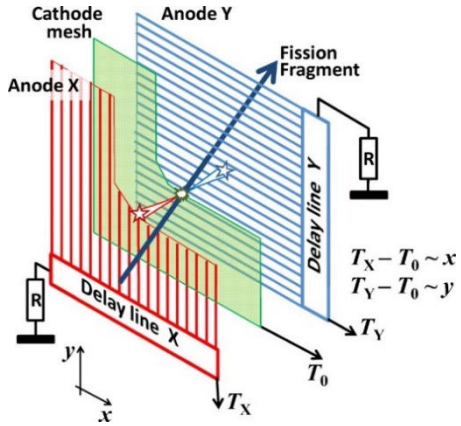

Fig. 2. Schema of the transparent position sensitive LPMWPC used in experiments.

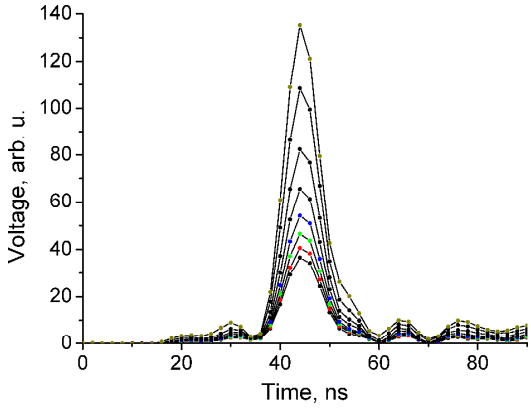

Fig. 3. Anode pulse shapes for 8 different incidence track angles: cos(θ) from 0.25 (biggest) to 0.95 (smallest).

2. Studies of the fission fragments angular distributions using LPMWPCs

Angular distributions of FFs and cross sections of nuclear neutron induced fission are the main source of information about fission barrier structure and nuclear transition states on the barrier. Such studies always were considered as a way to determine the transition states pa-

rameter, and an important tool to access the key characteristics and dynamics of the fission process. These data are not only of high scientific value, but of great significance for nuclear technologies as well. In our works [5,6] at the neutron time-of-flight spectrometer GNEIS [7] we have studied angular distributions of FFs in fission induced by intermediate energy neutrons for ^{232}Th, ^{235}U, ^{238}U, ^{233}U and ^{209}Bi.

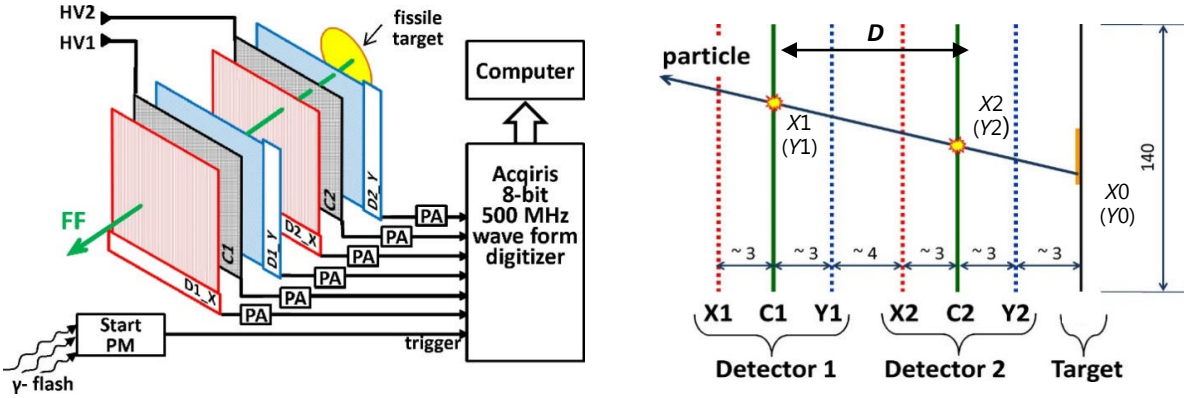

Fig. 4. Setup for studying of the fission fragments angular distributions. *D* is a distance between two cathodes.

The schema of the experimental setup based on two equal LPMWPCs detectors is shown in Fig. 4**.**.The LPMWPCs are placed close to each other and to the target in the beam in common stainless steel chamber filled with isobutane. The neuron beam is perpendicular to the detectors. FFs angle relative to the neutron beam can be derived easily from precise measurements of FFs positions on both detectors:

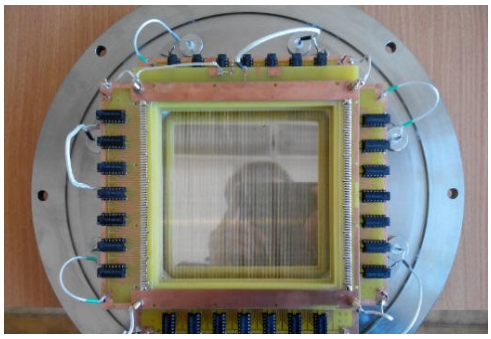

Fig. 5. Photo of the two LPMWPCs assembly.

$$\cos\theta = \frac{D}{\sqrt{(X1-X2)^2+(Y1-Y2)^2+D^2}}$$

We can also reconstruct fission position on the target (*X*0, *Y*0) using (*X*1, *Y*1) and (*X*2, *Y*2).

The neutron energy is determined by means of the conventional TOF-technique using the time difference between the trigger signal from gamma-flash START-detector (a “bare” photomultiplier inserted in the beam downwards the setup), and that from any of the cathode signals. A detailed description of the GNEIS spectrometer and neutron time-of-flight technique can be found elsewhere [7]. Signals from all 6 electrodes and the trigger signal from START-detector were recorded by 500 MHz waveform digitizer for further pulse height and time analyses. Photo of the LPMWPCs setup is shown in Fig. 5.

Test of the setup with ^{252}Cf isotopic source of fission fragments

For this test we used ^{252}Cf source having intensity ~10^4 fissions/s and circular shape with ⌀10 mm. The source was placed in front of the detector at the position of the targets for neutron induced fission. The measurements with the isotopic source were important for calibration of the angular efficiency of the setup. In this case trigger pulse was taken not from the accelerator, but from the cathode C1.

In Fig. 6 (left) a correlation of signal amplitudes from two cathodes is shown. Except the main diagonal locus, one can see the “line” with smaller C1 amplitudes attributed to events

that hit the cathode C1 mesh and did not penetrate into the last gap. They can be separated much better in a plot of cathode C1 amplitudes versus anode X1 amplitudes (last in stack), as shown in Fig. 6 (center). After applying the selection shown in Fig. 6 (center) by solid line, we get "clean" events for further analyses (see Fig. 6 (right)).

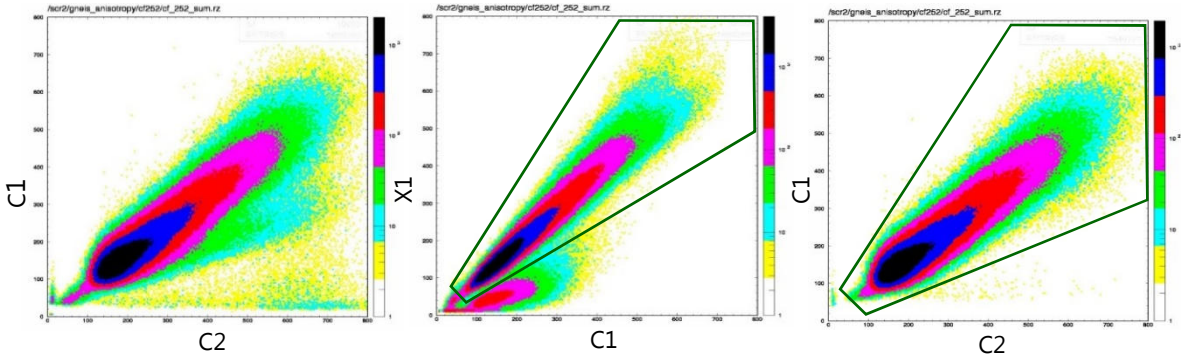

Fig. 6. Two-dimensional distributions of signal amplitudes from LPMWPC electrodes (see text).

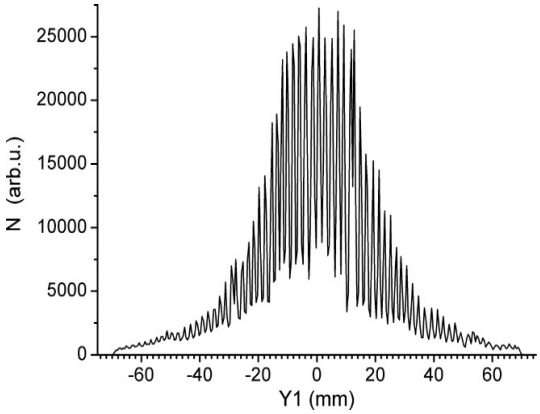

Fig. 7. Position distributions of FFs from ^{252}Cf source along Y axis of Detector 1.

Position distribution derived from time difference between anode and cathode signals for selected events is plotted in Fig. 7 (Y axis of Detector 1 is shown as an example). The timing resolution is better than the delay between adjacent wires (2 ns), so we can see grouping of events on individual wires. In Fig. 8 reconstructed distributions of fission events on the source in X and Y slices around the center are shown together with their Monte Carlo simulation in real geometry.

Ratio of numbers of events in main locus (N_0) and events with smaller amplitudes which hit wires of the last cathode C1 (N_1) in Fig.6 (center) is defined by transparency of the mesh cathode consisting of 2 wire planes. Total efficiency of the setup is defined by transparency of 7 wire planes which should be passed by fragment for to be registered in all planes. The total transparency correction factor can be estimated from experiment as:

$$k_t = \left(\frac{N_0 + N_1}{N_0}\right)^{\frac{7}{2}}.$$

The transparency factor is plotted in Fig. 9 as a function of angle together with the result of its calculation by Monte Carlo method with real wires geometry. It illustrates an accuracy of the geometry calculations in our Monte Carlo model.

Experimental distribution of $\cos\theta$ (W_{exp}) together with its Monte Carlo calculation in real geometry (W_{MC}) are shown in Fig. 10 (left). In Fig. 10 (right), the same distributions corrected for geometry factor $k_{\text{geom}} \sim 1/ W_{\text{MC}}$ are shown. We see that the after multiplying by k_{geom} the resulting corrected distribution (W_{corgeom}) is not uniform as expected for ^{252}Cf source. So additional correction had to be applied $k_{\text{d}} \sim 1/ W_{\text{corgeom}}$. This additional correction arises due to differential nonlinearity in position determination caused by characteristics of the delay line chips, and also due to signal cross-talk between channels. This correction obtained with the ^{252}Cf source was used in the measurements with other nuclei.

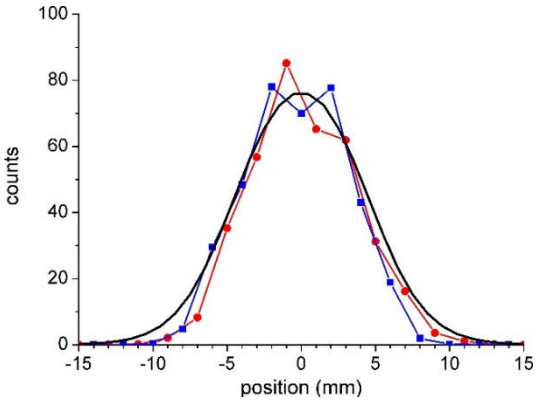

Fig. 8. Reconstructed distributions of fission events on ^{252}Cf source (⌀10 mm) in X and Y slices around the center (dots), and Monte Carlo simulation in real geometry (solid line).

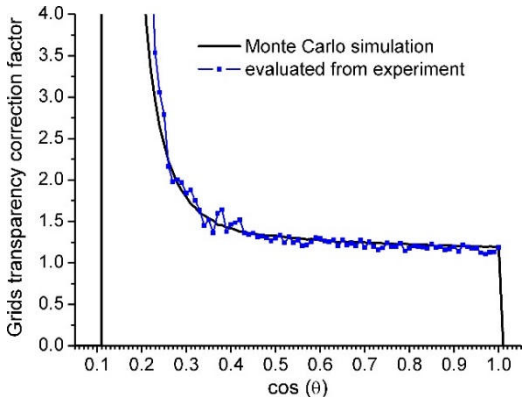

Fig. 9. Total grids transparency factor of the setup (see text).

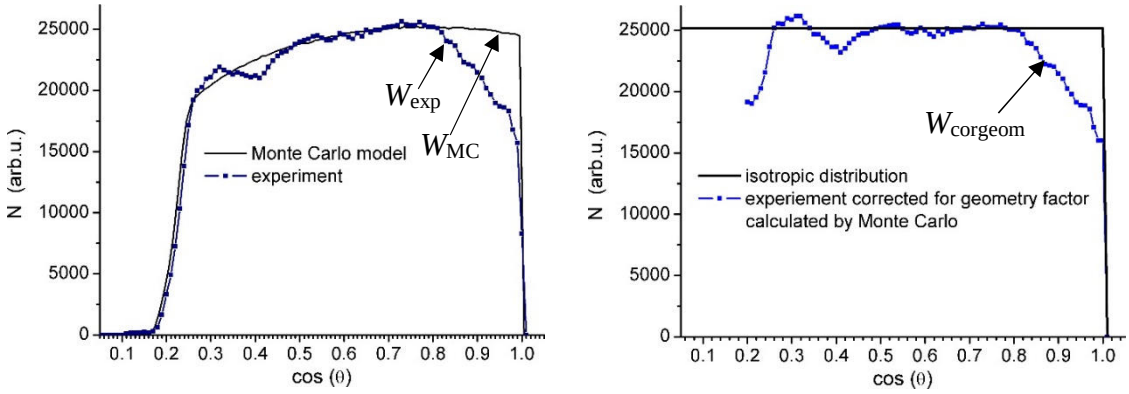

Fig. 10. Distribution of *cos θ* (see text).

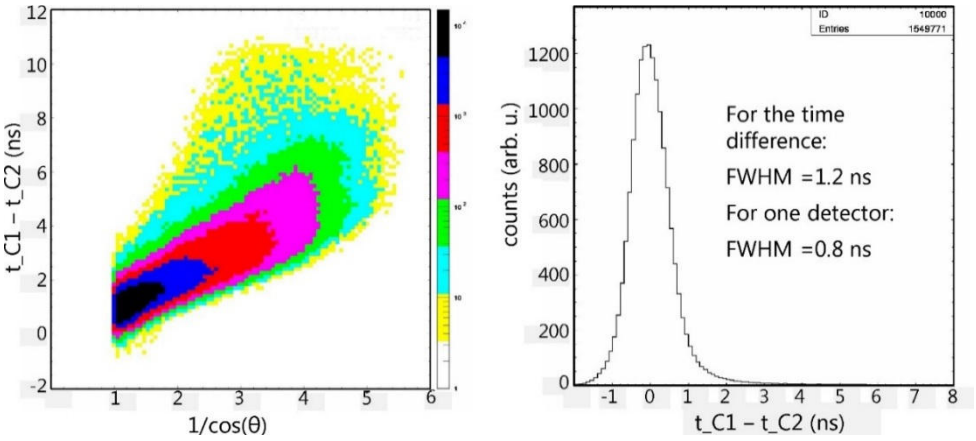

Fig. 11. Correlation of FFs time of fight between cathodes with 1/*cos θ* (left), projection of the two dimensional plot parallel to the line shown on the left part (right).

FFs time of flight between two cathodes over 1/*cos θ* is plotted in Fig.11 (left). One can see the anticipated linear correlation. On the right panel of Fig. 11, the projection of the two dimensional plot parallel to the axis line of the distribution (solid line on left panel) is shown. From this plot we can estimate time resolution of one detector as FWHM < 0.8 ns. It is upper estimation, because, practically, this line consists of two lines from light and heavy FFs separated ~0.6 ns at 1/ *cos θ* = 2.

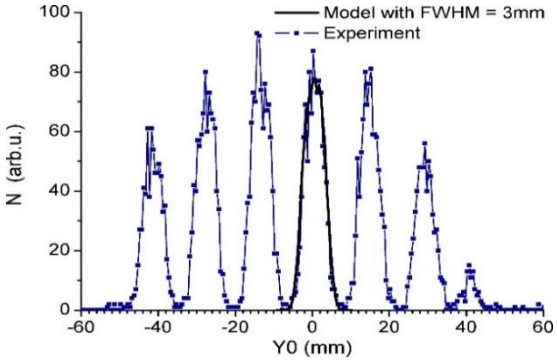

Fig. 12. Distribution of reconstructed fission positions on the ”multidot” target.

Tests with “multidot” ^{235}U target (neutron induced fission).

The next test was performed with special target made by vacuum deposition of ^{235}U tetrafluoride onto Mylar foil through shadow mask: 49 holes (grid 7 × 7) ⌀7 mm and equal spacing between columns and rows of 14 mm. In Fig 12, a reconstructed distribution of fission position on the target for central slice of the 7 × 7 pattern is shown. From this measurement we can estimate resolution for reconstructed position of fission on the target as 3 mm (FWHM).

Measurements of FFs angular distribution with 233U target (neutron induced fission).

The ^{233}U (oxide U_3O_8) was deposed on a 0.1 mm thick aluminum foil, shape of the active spot was rectangular 50 × 100 mm^2. Raw data were filtered for to remove non-fission events (noise, alpha particles from the target, recoil nuclei from target backing and surrounding materials) by applying the appropriate selection criteria in the correlated amplitude and time distributions. Reconstructed distribution of fission events on the target is shown in Fig. 13 (left). The shape is as one can expect for rectangular target irradiated with circular beam ⌀75 mm, which is shifted ~10 mm down due to some misalignment. It should be noted that there are no events outside the active spot rectangular (above and below) while these regions were in the neutron beam. This proves that there is no background from recoil nuclei coming from the target backing and constructing materials.

Experimental angular distribution summed over all neutron energies is shown in Fig. 13 (right) together with Monte Carlo simulation for isotropic FF emission. The experimental angular distributions for individual neutron energies intervals have been corrected for the geometry factor $k_{geom} \sim 1/ W_{MC}$ and also for additional correction factor k_d (related with differential nonlinearity) obtained as described in measurement with ^{252}Cf isotropic source.

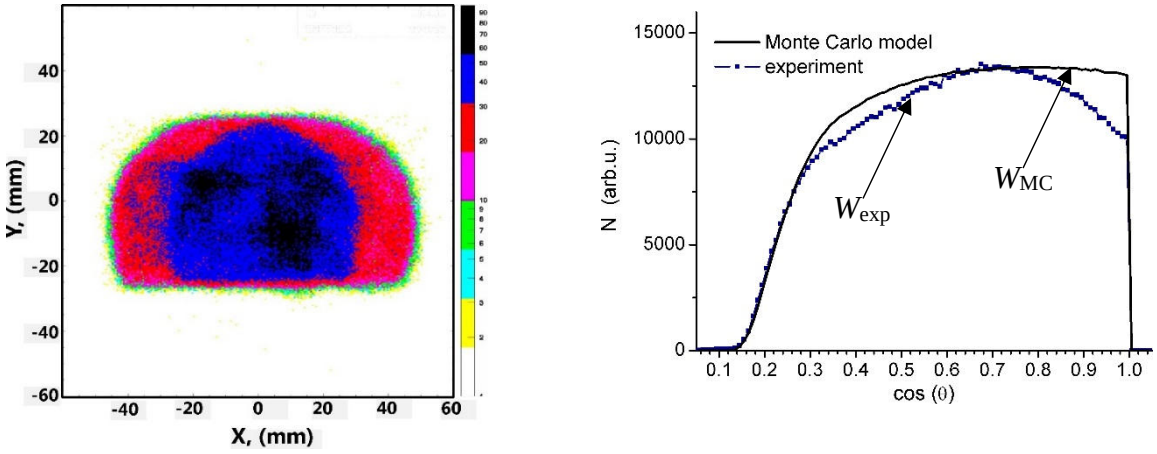

Fig. 13. Reconstructed distribution of fission events on the target (left); angular distribution summed over all neutron energies (right).

Examples of the corrected angular distributions for two neutron energies in comparison with formerly existing data [10,11] are presented in Fig. 14. The experimental data were fitted by sum of Legendre polynomials. The results of the completed analyses are published in [6].

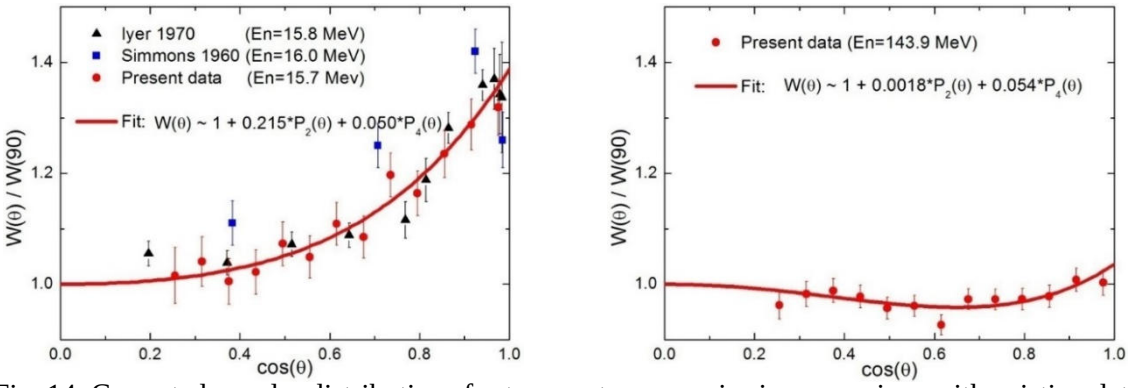

Fig. 14. Corrected angular distributions for two neutron energies in comparison with existing data [10,11] (dots). Result of fitting by sum of Legendre polynomials (line).

3. Measurement of the neutron beam spatial profile using the LPMWPCs

The facility for electronic components radiation hardness testing (ISNP/GNEIS) [8,9] has been created at neutron spectrometer GNEIS [7]. It was demanded to provide monitoring of the neutron beam intensity and profile with accuracy <10 % and position resolution <5 mm respectively.

It was obvious that the setup described above, equipped with sufficiently large and homogeneous fissile target, is perfectly suitable for this task. Also, it was decided to use somewhat simpler device with one LPMWPC. Scheme of the neutron beam profilometer is shown in Fig. 15. In this case, the target-converter with a size of 120 × 120 mm^2 is deposited on the common cathode made from 2 μm aluminized Mylar foil transparent for FFs. The converter material is ^{238}U with thickness ~500 μg/cm and uniformity <10%. Two complimentary FFs are emitted in approximately opposite directions, one fragment fixes X coordinate while the other - Y coordinate. The scheme is slightly differ from the device shown in Fig.2. Here we determine coordinates from time difference between signals from two ends of the anode delay line while the timing signal for neutron energy determination is taken from the cathode.

Neutron flux profiles with ⌀40 mm beam collimator for three neutron energies ranges are plotted in Fig 16. 2-dimentional neutron beam profile with ⌀75 mm collimator measured with the profilometer is shown in Fig. 17 (left). The results can be compared with the radiation dose profile measured with special dosimetry radiation sensitive film Gafchromic® EBT2 [12] (Fig. 17 (center)). Central slice of the beam profile obtained from the profilometer (dots) and from two independent photo scans of EBT2 film (lines) are compared in Fig. 17 (right).

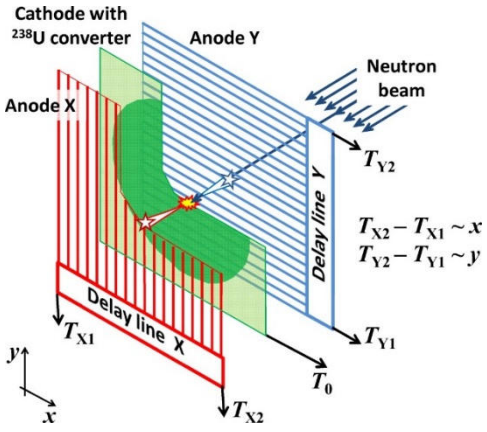

Fig. 15. Schema of the beam profilometer.

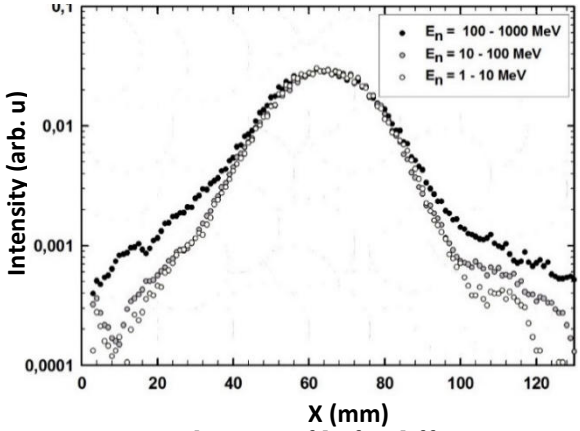

Fig. 16. Neutron beam profile for different energies.

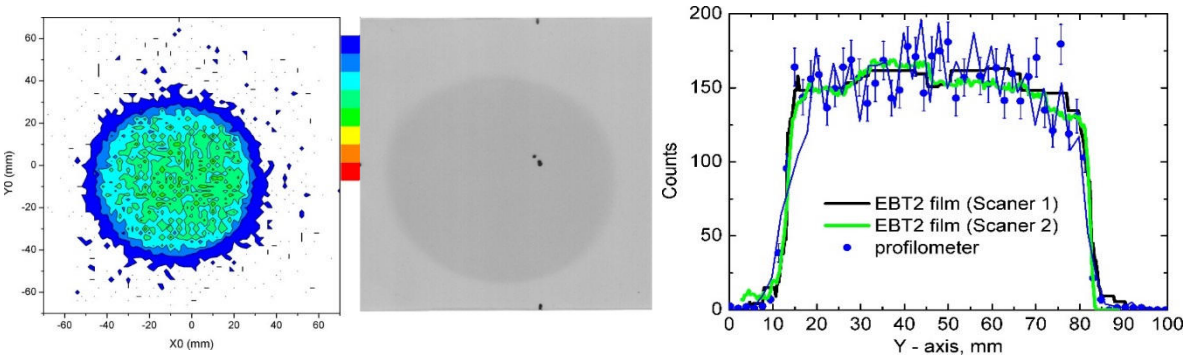

Fig. 17. Beam image from profilometer (left); scan of irradiated GAFCHROMIC® EBT2 film (center); central slice of the beam profile from profilometer and from two scans of EBT2 film (right).

4. Conclusions

Experimental setup based on two LPMWPCs was developed for measuring angular distributions of fission fragments. Angular anisotropy of FFs emission have been measured for for ^{232}Th, ^{235}U, ^{238}U, ^{233}U and ^{209}Bi [5,6]. The main parameters of the setup are:

Practically accessible θ angular range < 75^{o},
Efficiency at average angle ~80% (transparency of wires planes of two MWPCs),
Time resolution <0.8 ns,
Position resolution of reconstructed fission coordinates ~3 mm.

Neutron beam profile monitor was constructed based on LPMWPC with 238U converter deposited on the cathode. The profilometer was tested and now is exploited on the electronic components testing facility at neutron spectrometer GNEIS [8,9]. The main characteristics of the beam profile monitor are:

Area 140 × 140 mm^2
Position resolution ~2 mm
Time resolution <0.8 ns
Efficiency ~10^{-6} (with fission cross section σ_f ~1 barn)
Background <1%

References

1. G. Charpak, Ann. Rev. Nucl. Sci. **20**, 195(1970).
2. F. Binon et al., Nucl. Instrum. Methods **94**, 27 (1971).
3. A. Breskin, Nucl. Instrum. Methods **141**, 505 (1977).
4. A. Breskin, Nucl. Instrum. Methods Phys. Res. **196**, 11 (1982).
5. A.S. Vorobyev et al., JETP Letters **102**, 203 (2015).
6. A.S. Vorobyev et al., JETP Letters **104**, 365 (2016).
7. N. K. Abrosimov et al., Nucl. Instrum. Methods Phys. Res. A **242**, 121 (1985).
8. O.A. Shcherbakov et al., IEEE Trans. Nucl. Sci. **63,** 2152 (2016).
9. O.A. Shcherbakov et al., in *Proc. of the XXIII International Seminar on Interaction of Neutrons with Nuclei, Dubna, May 25–29, 2015* (JINR, Dubna, Russia, 2016), p. 214.
10. R. H. Iyer and M. L. Sagu, in *Proc. of the Nuclear Physics and Solid State Physics Symposium, December 27–30, 1970; Madurai, India: Nuclear Physics* 2 (Department of Atomic Energy, Government of India, Bombay, 1970), p. 57.
11. J. E. Simmons and R. L. Henkel, Phys. Rev.**120**, 198 (1960).
12. http://www.gafchromic.com/gafchromic-film/radiotherapy-films/EBT/index.asp